Rashba splitting in an image potential state investigated by circular dichroism two-photon photoemission spectroscopy

T. Nakazawa,[1] N. Takagi,[1] Maki Kawai,[1] H. Ishida,[2] and R. Arafune[3]
[1]*Department of Advanced Materials Science, University of Tokyo, Chiba 277-8561, Japan*
[2]*College of Humanities and Sciences, Nihon University, Tokyo 156-8550, Japan*
and Center for Materials Research by Information Integration, National Institute for Materials Science, Ibaraki 305-0047, Japan
[3]*International Center for Materials Nanoarchitectonics, National Institute for Materials Science, Ibaraki 305-0044, Japan*
(Received 1 December 2015; revised manuscript received 1 July 2016; published 7 September 2016)

We have explored the band splitting and spin texture of the image potential state (IPS) on Au(001) derived from the Rashba-type spin-orbit interaction (SOI) by using angle-resolved *bichromatic* two-photon photoemission (2PPE) spectroscopy in combination with circular dichroism (CD). The Rashba parameter for the first ($n = 1$) IPS is determined to be 48^{+8}_{-20} meV Å, which is consistent with the spin-polarized band structure calculated from the embedded Green's function technique for semi-infinite crystals. The present results demonstrate that bichromatic CD-2PPE spectroscopy is powerful for mapping the spin-polarized unoccupied band structures originating from SOIs in various classes of condensed matter.

DOI: 10.1103/PhysRevB.94.115412

I. INTRODUCTION

Spin-orbit interactions (SOIs) at solid surfaces and interfaces have attracted much attention [1–6], as the electron spin can be controlled through SOIs without magnetic materials. Optical excitation is a fascinating technique among the various methods proposed for handling the electron spin via SOIs, because it leads to the realization of logic operation devices based on fast spin control [7–12]. For the optical manipulation of the electron spin, the SOI in the unoccupied state is as important as that in the occupied state.

We chose circular dichroism (CD) measurements with two-photon photoemission (2PPE) spectroscopy [13–19] (CD-2PPE) for investigating the SOI characteristic in the unoccupied state of solid surfaces. CD-2PPE measurements yield different information in addition to the knowledge accumulated through the use of spin-resolved techniques such as spin-resolved 2PPE [20–24] and spin-resolved inverse photoemission [21,25–27], because CD reflects both the spin and orbital angular momenta [18,19] and the orbital angular momentum is as important as the spin angular momenta for investigating the SOI characteristics. Thus far, CD-2PPE has been used to measure the SOI characteristics in the photoexcited state on the surface of Heusler alloy [28] , Co thin films [29], and topological insulators [18,19]. Nevertheless, the CD data occasionally do not correlate directly to the spin character, because CD stems from both angular momenta. For example, Niesner *et al.* reported that the CD texture measured for Bi_2Se_3 with CD-2PPE does not agree with the expected spin texture [18]. For a deeper understanding of the CD-2PPE results, it is necessary to conduct CD-2PPE experiments for a simple system and analyze the SOI characteristics through detailed theoretical calculations. The image potential state (IPS) [13,15,30,31] offers a testing field to investigate the SOI in the unoccupied surface states, because it should be split by the Rashba-type SOI, which is well examined in the Shockley surface state (SS) [32–40]. The Rashba effect is a prototypical SOI due to inversion-symmetry breaking, and it results in spin-polarized bands: $E(k_\parallel) = E_{\mathrm{non-SOI}}(k_\parallel) \pm \alpha_R |k_\parallel|$, where α_R is the Rashba parameter and $k_\parallel$ is the electron momentum parallel to the surface [1,4,5]. The spin lies in the surface plane and remains perpendicular to $k_\parallel$ [Fig. 1(a)].

In order to confirm that the Rashba splitting in the IPS is definitely identified using CD-2PPE, one should demonstrate that (1) the CD signal stems from the unoccupied state, (2) the CD signal continuously increases with $k_\parallel$, and (3) the CD signal is consistent with the expected spin texture. Recently, Tognolini *et al.* [17] reported the Rashba splitting of the IPS on the graphene-covered Ir(111) surface by using CD-2PPE. They observed the CD signal in the *monochromatic* 2PPE spectra. Since the monochromatic 2PPE results are often affected by the occupied states, the bichromatic measurement is a prerequisite for determining whether the CD signature originates from the unoccupied states.

In this work, we present compelling results proving that the band splitting due to the Rashba effect in IPS is characterized using CD-2PPE spectroscopy. We also present a theoretical analysis based on a density functional theory (DFT) code employing the embedded Green's function (EGF) technique [39,41,42]. To fulfill the above-mentioned criteria, we have conducted *bichromatic* CD-2PPE experiments [Fig. 1(b)] with high energy resolution and used two experimental geometries to ensure consistency between the CD signature and the spin texture. We chose Au(001) - (5×20) as the sample for our first demonstration of bichromatic CD-2PPE spectroscopy. (Hereafter, we refer to this surface as simply Au(001) for the sake of brevity.) Its electron spin degenerates in the occupied states immediately below the Fermi level, enabling us to identify clearly the CD signal with the unoccupied state origin.

II. EXPERIMENTAL AND CALCULATIONAL DETAILS

The experiments were performed using a laser system based on a narrow-bandwidth Ti:sapphire laser oscillator (Coherent, Mira900) as the excitation source and a hemispherical electron energy analyzer (Specs GmbH, Phoibos 100) equipped with a two-dimensional CCD detector. The laser pulse duration was 2.0 ps and the repetition rate was 80 MHz. The photon energy was set at 1.654 eV. A fraction of the IR pulse

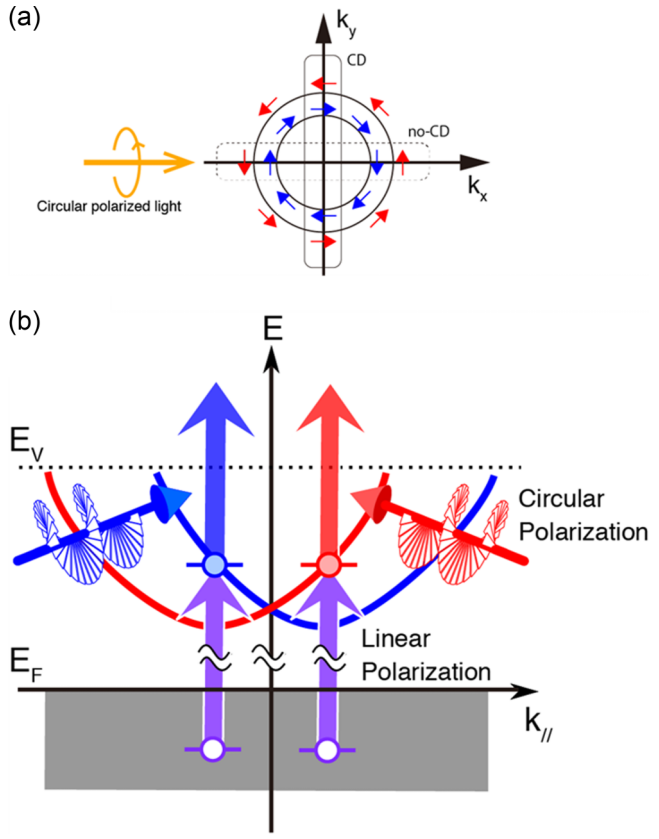

FIG. 1. (a) Rashba-type spin texture. This spin texture is expected in the IPS of Au(001). The experimental geometry for measuring the electrons surrounded by the solid line allows for CD, while the other geometry corresponding to the dotted line does not. (b) Schematic energy diagram for CD-2PPE. The helicity of the IR polarization determines the spin direction of the electrons excited preferentially.

was frequency tripled using nonlinear crystals to produce UV (4.962 eV) light. The laser power was 8 mW for the UV light and 460 mW for the IR light. The p-polarized UV pulse excited the electrons from the occupied states to the unoccupied states without spin selectivity, while the circular polarized IR pulse caused the electrons in the unoccupied state to be emitted into vacuum, depending on its spin polarization. The circularity of the polarization was 91%. Both the pump and the probe laser beams were aligned collinearly using a dichroic mirror and focused onto the sample in a spot with a diameter of approximately 100 μm using an achromatic lens (f = 350 mm). The ultrahigh vacuum chamber was made of μ metal and had a base pressure better than 1.0×10^{-10}mbar. The sample temperature was 11 K during the 2PPE measurements. The total energy resolution was maintained at 9.5 meV. The momentum resolution was better than 0.01Å^{-1}. The clean Au (001)–(5 × 20) surface was obtained by cycles of Ar ion sputtering (600 eV, 30 min) and annealing (20 min at 740 K). The (5 × 20) reconstruction is judged from the low-energy electron diffraction (LEED) pattern.

We have used two experimental geometries to ensure consistency between the CD signature and the spin texture as shown in Fig. 2. The difference between them is the difference in the emission plane with respect to the incident plane. The

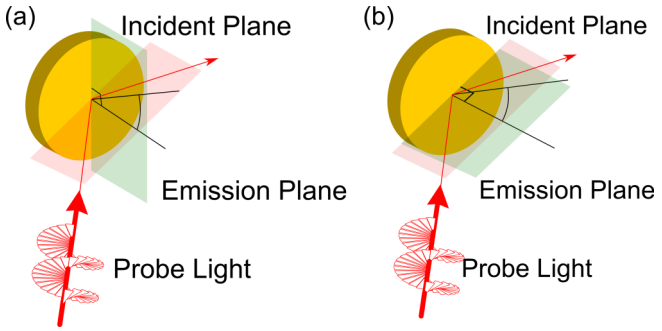

FIG. 2. The emission geometries in the current work. (a) The emission plane is perpendicular to the incident plane. (b) The emission plane is parallel (identical) to the incident plane. While (a) corresponds to the data shown in Fig. 3, (b) is for Fig. 4.

emission plane includes the surface-normal direction in both geometries. Recalling that the CD signal does not appear when the light wave vector is perpendicular to the spin direction [43], we have measured the CD-2PPE spectra along the k_x and k_y directions. Here, the x axis is parallel to the incident plane of the light and the surface plane, and the z-axis the surface normal. The appearance of CD should depend on the emission geometry when CD originates from the Rashba effect; the CD signal does not appear in the measurement along the k_x direction, because the spin texture is chiral, as shown in Fig. 1(a).

The electronic structure of semi-infinite Au(001) was calculated within DFT by using a computer code [41] that combines the surface EGF technique of Inglesfield [44] and the full-potential linearized augmented plane-wave (LAPW) method [45]. We have assumed Au(001) without the surface reconstruction; we have calculated the electronic band of the semi-infinite Au(001)-1 × 1. In this code, the spin-orbit (SO) coupling is implemented only within the muffin-tin (MT) spheres centered at each atom. This approximation is justified since, as estimated by McLaughlan *et al.* [34], the Rashba splitting of the IPSs arising from the potential gradient in the vacuum region is only of the order of 0.01 meV.

To be able to describe a series of the IPSs, the short-ranged DFT surface barrier potential on the vacuum side of the outermost atomic layer is replaced by a model image potential [46],

$$V(z) = E_v - \frac{e^2}{4|z - z_{im}|}, \quad (1)$$

using a smooth interpolation function, where E_v denotes the vacuum level and z_{im} is the normal coordinate of the image plane. We used the same E_v value as that obtained from the DFT calculation of the neutral surfaces. On the other hand, we determined z_{im} as the centroid of the screening charge density induced by a uniform electric field perpendicular to the surface. The calculated values of E_v and z_{im} within the local density approximation (LDA) are 5.50 eV (relative to the Fermi energy, i.e., the work function) and 2.67 bohrs (relative to the outermost atomic plane). The corresponding ones within the generalized gradient approximation (GGA) are 5.07 eV and 2.72 bohrs, respectively. By calculating the Green's function of the semi-infinite surface having the surface barrier potential

modified in this way, we investigated the energy dispersions of surface states with $k_{\parallel}$ as well as their spatial distributions and spin polarizations. In the present paper, we show mainly the results based on the LDA + model image potential, since the E_v value within the LDA agreed better with the experimental one.

III. RESULTS AND DISCUSSION

Figure 3(a) shows the angle-resolved 2PPE spectra of the Au (001) surface. The measurement geometry is shown in Fig. 2(a); the emission plane was substantially normal to the incident plane. The spectra in green and orange were probed by the left- and right-circularly polarized (LCP and RCP) light, respectively. In both helicities (LCP and RCP) the parabolic band appeared, which confirms that the observed peaks originate from the IPS. The binding energy of the band at the $\bar{\Gamma}$ point were determined to be 745 ± 0.5 meV measured from the vacuum level (E_V) and $0.73 \pm 0.05\, m_0$(m_0 is the mass of a free electron), respectively, by assuming a single parabolic band. The binding energy at the $\bar{\Gamma}$ point and the effective masses were independent of the light helicity. The FWHM at the $\bar{\Gamma}$ point was 42.0 meV: the intrinsic width was determined to be 40.9 meV, after accounting for the effect of the instrumental resolution. The binding energy of $n = 1$IPS on Au(001) has been reported: 0.63 eV [47]. We believe that the discrepancy between the current result and the reported value stems mostly from the insufficient energy resolution and inaccuracy in the work-function determination in the previous work [48]. The binding energy of IPS is generally described as $\frac{0.85\ \text{eV}}{(n+a)^2}$, where a is called the quantum defect and is related to the relative energy within the energy gap; $a = 0-0.5$ from top to bottom of the band gap [15]. The value of 0.745 eV corresponds to $a = 0.07$, which is consistent with our calculation showing the IPS is located near the top of the energy gap. (The energy band is shown below.) The reported value [49] of the effective mass ($1.5 \pm 0.3\, m_0$) is also different from the current result. We surmise that this discrepancy originates from the improvement in the energy and momentum resolutions. We also note that the effective mass we measured is low for IPS, which is nearly unity for most surfaces. An exceptionally light effective mass is reported for IPS on W(110) [50].

Figure 3(b) shows the 2PPE spectra measured at $k_{\parallel} = -0.162$, 0, and $0.173\ \text{Å}^{-1}$ to highlight the circular dichroic difference. By analyzing the spectral shapes carefully, we found that there was a slight but significant degree of CD. The peak position for the RCP light (orange curve) was slightly higher than that for the LCP light (green curve) when $k_{\parallel} < 0$ [upper panel of Fig. 3(b)]. Figure 3(c) shows the peak positions as a function of $k_{\parallel}$. The peak positions exhibit a disparity depending on the helicity of the probe light; the peak position for the LCP light is higher than that for the RCP light on the positive side of $k_{\parallel}$, while the peak positions are reversed on the negative side.

Figure 4(a) shows the angle-resolved 2PPE spectra measured with another geometry; the emission plane is identical with the incident one [Fig. 2(b)]. The binding energy and the

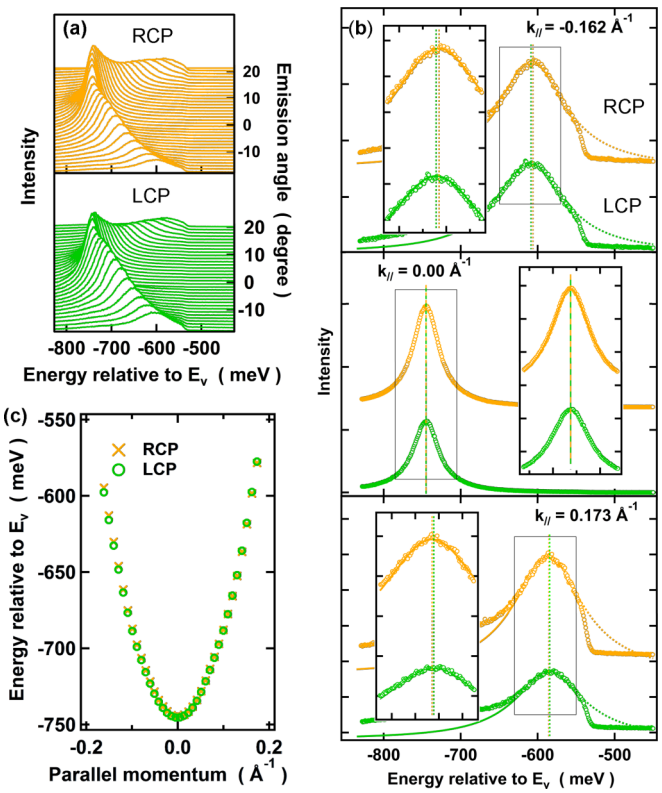

FIG. 3. Spectroscopic data for CD-2PPE experiments on Au(001). (a) All the data for the angle-resolved 2PPE spectra of Au(001). The upper (lower) panel shows the data probed by the RCP (LCP) light. (b) CD-2PPE spectra of Au(001). The dotted curve denotes the Lorentz function fit that determines the peak position. The inset in each panel shows a magnified view of the rectangular area to highlight the difference in peak positions. (c) The peak position versus $k_{\parallel}$. The green circles (orange crosses) are the results corresponding to the LCP (RCP) light.

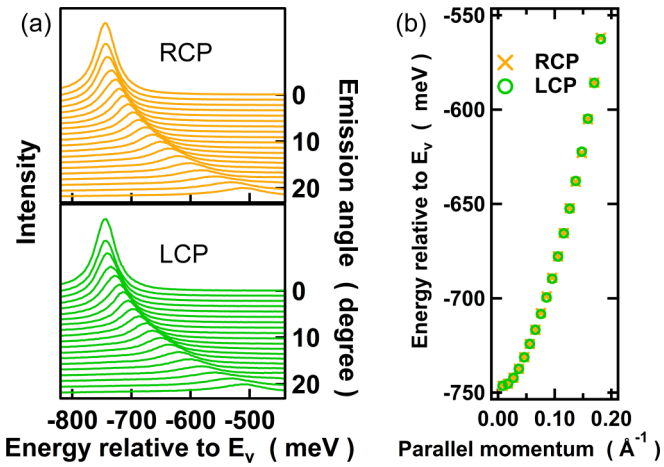

FIG. 4. CD-2PPE spectra of Au(001) when the emission plane includes the incident plane. (a) Angle-resolved CD-2PPE spectra of Au(001). The upper panel shows the data probed by the RCP light, while the lower panel shows the data probed by the LCP light. (b) The peak position versus the parallel momentum. The orange circles are the results corresponding to the RCP light, and the green crosses are from the LCP light.

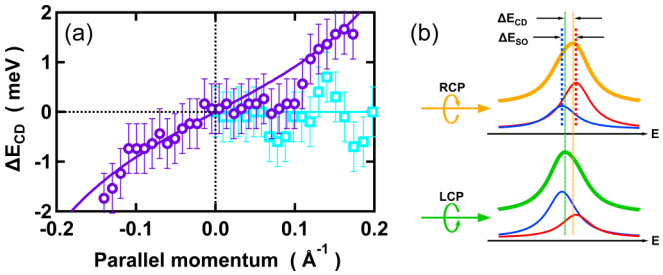

FIG. 5. Peak position disparity due to the light helicity. (a) ΔE_{CD} versus $k_{\parallel}$. The purple circles are the data from Fig. 2(d). The experimental uncertainty for ΔE_{CD} measurement is ± 0.5 meV. The purple curve is the fitted result for the intensity ratio $(I_{\uparrow}/I_{\downarrow})$ of 0.88 under $\alpha_R = 48$ meV Å (see text). The sky-blue squares denote the results for when the emission plane is identical to the incident plane. No circular dichroism appeared in this case. (b) Schematic view of the measured spectra. The orange and green curves are the spectra measured using the RCP and LCP probe lights, respectively. These spectra are deconvoluted using the intrinsic components of the spin-orbit splitting bands (blue and red curves).

effective mass are the same in both geometries. As shown in Fig. 4(b), the CD did not appear with this measurement geometry.

Figure 5(a) summarizes the results of the circular dichroic difference ΔE_{CD}, which is defined as the difference between the peak position for the RCP light and that for the LCP light. ΔE_{CD} increases with the increase in $k_{\parallel}$ for the emission plane perpendicular to the incident plane. On the other hand, when both the incident and emission planes are identical, ΔE_{CD} does not show a systematical dependence on $k_{\parallel}$ and thus $\Delta E_{\mathrm{CD}} = 0$ essentially. This indicates that the spin lies in the surface plane and is perpendicular to $k_{\parallel}$. The observed CD distribution confirms that the Rashba split in the IPS is definitely measured using angle-resolved CD-2PPE spectroscopy. Therefore, we have concluded that the Rashba effect in the IPS on Au(001) is identified using CD-2PPE spectroscopy.

Now, let us determine α_R from the $k_{\parallel}$ dependence of ΔE_{CD}; $\alpha_R = \frac{\Delta E_{SO}}{2|k_{\parallel}|}$, where ΔE_{SO} is the spin-orbit splitting. Note that ΔE_{SO} significantly differs from ΔE_{CD} as shown in Fig. 5(b) (Appendix A). From the curve of Fig. 5(a), one can also see that $\Delta E_{\mathrm{CD}} \neq \Delta E_{SO}$; the curve also shows that the $k_{\parallel}$ dependence of ΔE_{CD} is not linear, even though ΔE_{SO} is linear to $k_{\parallel}$. In order to determine ΔE_{SO} and thus α_R, we fitted the spectra with two homothetic Lorentz peaks; the separation between these two peaks is ΔE_{SO}, and their intensities $(I_{\uparrow}, I_{\downarrow})$ depend on the light helicity. We have obtained $\alpha_R = 48^{+8}_{-20}$ meV Å and $I_{\uparrow}/I_{\downarrow} = 0.88^{+0.05}_{-0.16}$ by using the least-squares fit [the solid curve in Fig. 5(a)]. Incidentally, the effect of the deviation from the perfect circular polarization of the light was buried under the fitting uncertainty. The Rashba split of the IPS on Au(001) was predicted by McLaughlan *et al.* [34]. They used the relativistic multiple-scattering theory and calculated α_R to be 44 meV Å, which agrees well with our fitting results.

Since CD is not the direct proof for the spin texture, we ensured that the CD in our results is certainly derived from the spin texture with the aid of calculations. Figure 6(a) shows the intensity plot of the k-resolved density of states (DOS)

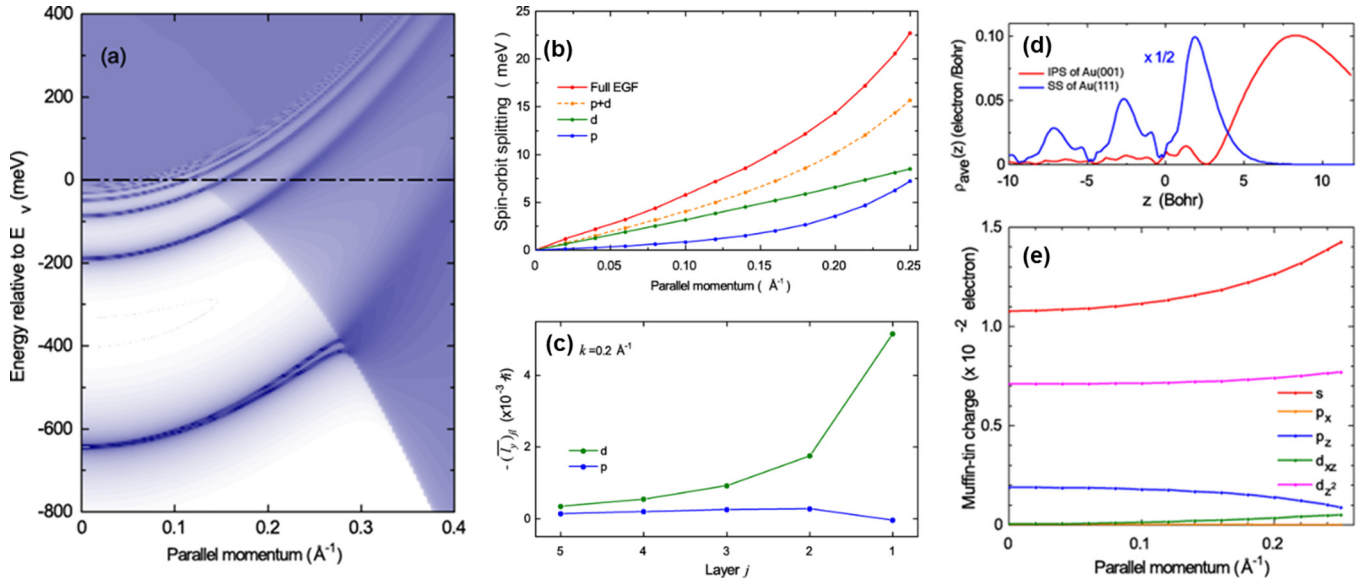

FIG. 6. Theoretical calculation results. (a) Electronic band structure of Au(001) along the $\bar{\Gamma} - \bar{X}$ direction determined by a first-principles calculation based on the embedded Green's function technique. (b) Spin-orbit splitting (ΔE_{SO}) of the image potential state with $n = 1$ on Au(001) along the $\bar{\Gamma} - \bar{X}$ direction (red line). Blue and green lines show the p- and d-orbital contributions to $\Delta E_{SO}(k_{\parallel})$ evaluated by Eq. (5). (c) The y component of orbital angular momentum (OAM) in a MT sphere of surface atoms with radius 2.48 bohrs averaged over two spin-split bands of the image potential state with $n = 1$ on Au(001) at $k_{\parallel} = 0.2$ Å^{-1} as a function of layer index. The blue and green lines show the contributions of the p and d orbitals, respectively. (d) Planar averaged charge density $\rho_{\mathrm{ave}}(z)$ of the lowest IPS on Au(001) (red line) and the corresponding one of the SS for Au(111) (blue line) as a function of the normal coordinate z, which is measured relative to the outermost Au plane. (e) Orbital-decomposed charges of the lowest IPS within the muffin-tin sphere of the first-layer Au atom (radius 2.48 bohrs) as a function of $k_{\parallel}$.

calculated in a first-layer MT sphere with radius 2.48 bohrs along the $\bar{\Gamma}-\bar{X}$ line. The bright region corresponds to a projected bulk band gap, while the dark-colored regions on the higher-energy sides are projected bulk bands of Au, except for the parabolic region, $E-E_v \geqslant \frac{(\hbar k_\parallel)^2}{2m_0}$, which corresponds to the projection of the energy continuum of the semi-infinite vacuum. The full series of IPSs ($n = 1, 2,...$) appeared inside the projected band gap at the $\bar{\Gamma}$ point, exhibiting free-electron-like parabolic energy dispersions with $k_\parallel$. With the combination of LDA and a model image potential, we obtained 648 meV and 1.08 m_0 as the binding energy and effective mass of the lowest image potential state ($n = 1$) at the $\bar{\Gamma}$ point, respectively. These values agree well with those in a previous calculation of McLaughlan *et al.* [34]. On the other hand, unfortunately, the calculation does not reproduce the light effective mass measured. One of the possible reasons for this discrepancy may be the fact that we did not consider the surface reconstruction. Taking into account the surface reconstruction, it would be possible to match the calculated band structure to the experimental data including the Rashba parameter. The red line in Fig. 6(b) shows $\Delta E(k_\parallel)$, the energy difference between the two spin-split image potential states with $n = 1$ as a function of $k_\parallel$ along the $\bar{\Gamma}-\bar{X}$ direction. While $\Delta E(k_\parallel)$ increases linearly at small $k_\parallel$, the deviation from linear dependence becomes increasingly more visible with increasing $k_\parallel$.

The energy splitting of the image potential state is caused by the SO coupling term,

$$\hat{H}_{so} = f_{so}(r)(\vec{l}\cdot\vec{\sigma}), \tag{2}$$

which is nonvanishing in a small space surrounding each nucleus. Here, $f_{so}(r)$ is a radial function involving the radial derivative of the LDA potential energy [39], $\vec{l}$ is the orbital angular momentum (OAM) operator, and $\vec{\sigma}$ denotes the Pauli matrix. The OAM associated with the image potential state vanishes at the $\bar{\Gamma}$ point. When $k_\parallel$ is oriented in the positive x direction, the y component of the OAM of surface atoms starts increasing in the negative direction with increasing $k_\parallel$. As a result, $\hat{H}_{so}$ splits the spin-degenerate image potential state into the upper band whose spin is polarized in the negative y direction and the lower one whose spin is polarized in the positive y direction. Here, it is important that the above-mentioned y component of the OAM does not arise due to SO coupling. Instead, it originates from the symmetry breaking at the surface and already exists in the scalar-relativistic wave function. Actually, it turned out that the y component of the OAM for the spin-degenerate image potential state calculated without $\hat{H}_{so}$ is nearly the same as the corresponding one for the full relativistic wave function averaged over the two spin-split states.

Within a perturbation theory, the spin-orbit splitting of the image potential state may be approximated as

$$\Delta E_{SO} \approx \langle\psi_+|\hat{H}_{so}|\psi_+\rangle - \langle\psi_-|\hat{H}_{so}|\psi_-\rangle, \tag{3}$$

where ψ_+ and ψ_- denote the wave functions of the upper and lower bands, respectively. In the LAPW method, these wave functions are expressed within the MT sphere of atom j as

$$\psi_\pm \approx \sum_{l,m}[c_{\pm jlm}u_{jl}(r) + d_{\pm jlm}\dot{u}_{jl}(r)]Y_{lm}\begin{pmatrix}1/\sqrt{2}\\ \mp i/\sqrt{2}\end{pmatrix}, \tag{4}$$

where u_{jl} denotes the normalized radial basis function, $\dot{u}_{jl}$ is its energy derivative, and we choose the y axis as the quantization axis of spherical harmonics Y_{lm}. For simplicity, let us neglect the smaller contribution containing $\dot{u}_l$. Then, substituting Eq. (4) into Eq. (3) and noting that ψ_+ and ψ_- are spin polarized in the negative and positive y directions, respectively, we obtain

$$\Delta E_{SO} \approx -\sum_j\sum_l\langle u_{jl}|f_{so}|u_{jl}\rangle[\langle l_y\rangle_{+jl} + \langle l_y\rangle_{-jl}], \tag{5}$$

where

$$\langle l_y\rangle_{\alpha jl} = \sum_m m|c_{\alpha jlm}|^2 \tag{6}$$

is the y component of the OAM of atom j for band α decomposed into azimuthal quantum number l.

The blue and green lines in Fig. 6(b) show the contribution of the p ($l = 1$) and d ($l = 2$) orbitals to the spin-orbit splitting $\Delta E_{SO}(k_\parallel)$ evaluated by Eq. (5). The contribution of higher angular momentum states is negligibly small. As is seen, at small $k_\parallel$, the spin splitting of the two bands is mainly caused by the d-orbital components of the wave function. Furthermore, the contribution of the d states increases nearly linearly up to large $k_\parallel$ values. On the other hand, the p-state contribution increases more than linearly and becomes comparable with the d-state contribution at large $k_\parallel$. The dashed line in Fig. 6(b) shows the sum of the two orbital contributions. α_R is evaluated to be 29.5 meV Å from the energy splitting at small $k_\parallel$ (<0.14 Å^{-1}). For larger $k_\parallel$, the energy splitting exhibits a nonlinear behavior. These features agree well with the IPS bands reported by McLaughlan *et al.* [34]. The fact that this line underestimates $\Delta E_{SO}(k_\parallel)$ of the full EGF calculation reveals the limitation of the perturbation treatment Eq. (3). That is, the kinetic-energy and potential-energy parts of the Hamiltonian also make a certain contribution to $\Delta E(k_\parallel)$, since the spatial part of the full relativistic wave functions, ψ_+ and ψ_-, are not identical. Finally, we show in Fig. 6(c) the y component of the OAM averaged over two bands, $\langle\overline{l_y}\rangle_{jl} = (\langle l_y\rangle_{+jl} + \langle l_y\rangle_{-jl})/2$, at $k = 0.2$ Å^{-1} as a function of layer index. As is seen, $\langle\overline{l_y}\rangle_{jl}$ of the d states exhibits the largest amplitude on the outermost surface layer and decays monotonously toward the interior of the metal. On the other hand, $\langle\overline{l_y}\rangle_{jl}$ of the p states changes its sign between the first and second layers. It has the largest amplitude on the second surface layer. While the magnitude of $\langle\overline{l_y}\rangle_{jl}$ for the p orbital is seen to be much smaller than that of the d orbitals, the p-state contribution to $\Delta E_{SO}(k_\parallel)$ becomes about half of the d-state contribution at $k = 0.2$ Å^{-1}, since the matrix element $\langle u_{jp}|f_{so}|u_{jp}\rangle$ is by more than 4 times larger than $\langle u_{jd}|f_{so}|u_{jd}\rangle$.

It would be interesting to compare our result with that for the SS of Au(111) investigated with CD–angle-resolved photoemission spectroscopy (ARPES) measurements [38]. There are two differences between them; one is the large difference in

α_R ($\alpha_R = 330$ meV Å for the SS of Au(111) [35]). The other is that the current CD-2PPE results are consistent with the expected spin texture while the CD distribution measured with CD-ARPES does not match with the spin texture determined through spin-resolved ARPES experiments. We assigned these differences as the difference in the OAM contribution by using DFT calculations with the EGF technique. Figure 6(d) compares the planar averaged charge density calculated for the lowest IPS at $\bar{\Gamma}$ with that for the SS on Au(111). In the interior of the crystal, the former is smaller than the latter nearly by an order of magnitude. In fact, as seen from Fig. 6(e), the sum of the orbital-decomposed charges in a sphere surrounding the first-layer Au atom (primarily the s, p_z, and d_{z2} components) is as small as ~0.02 electrons for the lowest IPS at $\bar{\Gamma}$, while the corresponding one amounts to ~0.18 electrons for the SS on Au(111). This explains why α_R for the IPS on Au(001) is smaller than that for the SS on Au(111).

The difference between the CD distribution of the SS on Au(111) and the IPS on Au(001) is rationalized by the difference in contributions from the orbital moment to the CD signals. The contrast arises from the fact that CD cannot fundamentally distinguish between the spin and the orbital angular momenta, and implies that the contribution from the spin and orbital angular momenta to the CD signal taken for the IPS is different from that for the SS. In fact, the orbital angular momentum for the IPS is an order of magnitude smaller than that for the SS. The contribution from the d orbital is much smaller for the IPS than that for the SS. This means that the spin angular momentum accounts significantly for the total angular moment in the IPS. Thus, we have concluded that the measured CD signal corresponds with the spin direction in IPS.

Before closing the discussion, we would like to point out that it would be interesting to explore materials that exhibit a large difference between $I_\uparrow$ and $I_\downarrow$, because it leads to a substantial spin-polarized photocurrent. McIver *et al.* [10] reported that the photocurrent for Bi_2Se_3 changes because of the polarization of the incident light through its helical Dirac dispersion. If one were to prepare a solid surface with strongly spin-polarized bands in both the occupied and unoccupied states, the surface would give rise to a large intensity asymmetry in CD. We believe that CD-2PPE would be useful for finding such materials.

Last, we comment on the work of Tognolini *et al.* [17]. As mentioned above, they equated ΔE_{CD} to ΔE_{SO}, which can provide an inaccurate (too small) Rashba parameter. However, their determined value reasonably matched with the theoretical value. Indeed, their measured ΔE_{CD} is larger than our values by an order of magnitude. It might be meaningful to identify what causes the difference between their work and ours even though the samples are different from each other. We believe that the CD signal originates from the occupied states in their work. They measured the *monochromatic* CD-2PPE spectra. It is difficult to distinguish whether the spectral signature arises from the occupied or unoccupied state from the *monochromatic* experiments. It should be noted here that the photon energy in their experiments (4.64 eV) agrees with the energy difference between the IPS and the spin-polarized surface resonance of Ir(111). If they had measured the *bichromatic* CD-2PPE spectra with different emission geometry, one could have elucidated the origin of the CD signal.

IV. SUMMARY

We have measured the angle-resolved bichromatic 2PPE spectra of Au(001) with circularly polarized light in order to identify the band splitting due to the Rashba effect in the IPS. A careful analysis based on DFT calculations performed using the EGF technique confirmed that CD-2PPE experiments certainly probe the Rashba splitting in the IPS on the Au(001) surface. The obtained results demonstrate that the CD technique and high-resolution 2PPE spectroscopy are useful for measuring the SOI-induced band split, even when it is buried in the broad intrinsic linewidth. We expect that this technique will contribute to the quest for materials that exhibit large spin-polarized photocurrents.

ACKNOWLEDGMENTS

This work was supported by JSPS KAKENHI Grants No. 15K13506, No. JP2511006, and No. JP2511008, and the World Premier International Research Center Initiative (WPI) on Materials Nanoarchitectonics (MANA).

APPENDIX A: CIRCULAR DICHROIC DIFFERENCE AND SPIN-ORBIT SPLITTING

In this Appendix, we would like to point out that the spin-orbit splitting (ΔE_{SO}) is not equal to the circular dichroic difference (ΔE_{CD}). The left panel of Fig. 7 is the simulated CD spectra when the intensity ratio ($I_\uparrow : I_\downarrow$) is 5:4, where $I_\uparrow$ and $I_\downarrow$ are the peak intensities of the up-spin and down-spin bands probed by the RCP light, respectively. When ΔE_{SO} is smaller than the linewidth (ω), ΔE_{SO} significantly differs from ΔE_{CD} that is measured directly [the upper spectra in Fig. 4(c)]. It is only when ΔE_{SO} is comparable to (or larger

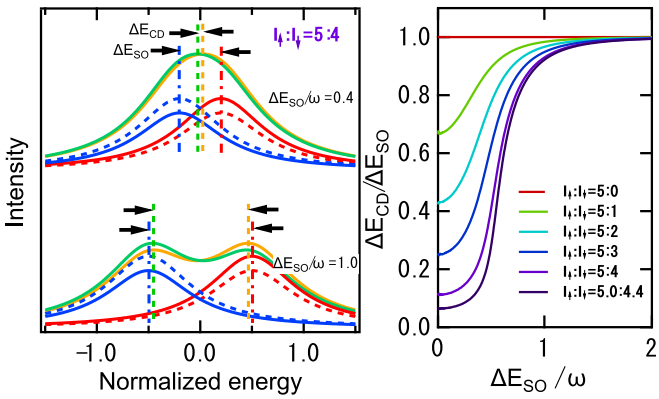

FIG. 7. (Left) Simulated CD spectra when the intensity ratio ($I_\uparrow : I_\downarrow$) is 5:4. The orange and green curves are the spectra corresponding to the RCP and LCP probe lights, respectively. The solid (dotted) red and blue curves are deconvoluted spectra of the spin-polarized bands for RCP (LCP) light, respectively. The energy is normalized by the FWHM (ω) of the deconvoluted spectrum (red or blue). $\Delta E_{SO}/\omega$ is 0.4 for the top spectra and 1.0 for the bottom spectra, where ΔE_{SO} is the spin-orbit splitting width and ω is the intrinsic linewidth of the spin splitting bands. (Right) $\Delta E_{SO}/\omega$ versus $\Delta E_{\mathrm{CD}}/\Delta E_{SO}$. These figures clearly show that ΔE_{CD} is smaller than ΔE_{SO}, and the difference cannot be ignored when ΔE_{SO} is smaller than ω.

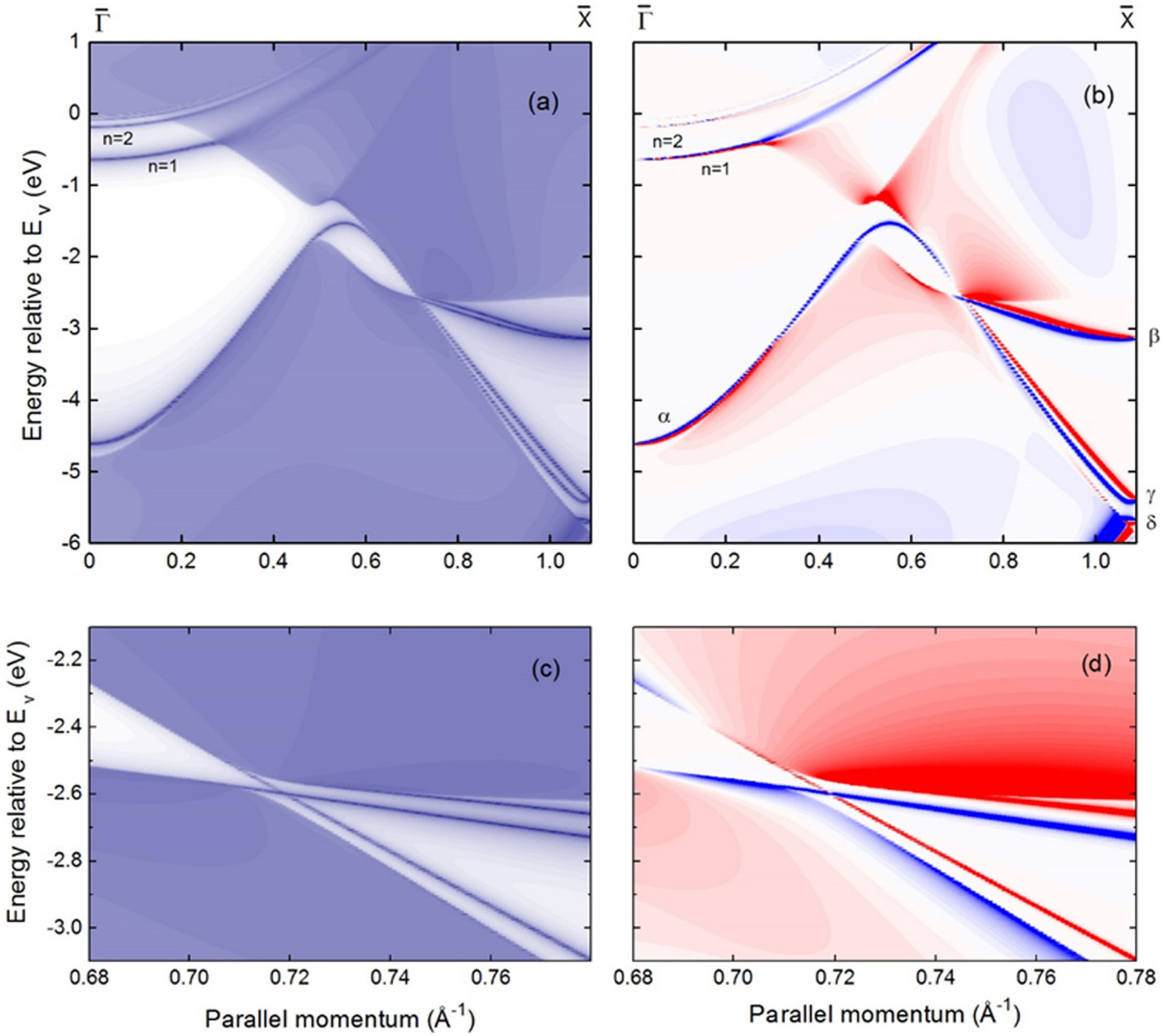

FIG. 8. (a) Intensity plot of k-resolved DOS calculated in a first-layer MT sphere with radius 2.48 bohrs for semi-infinite Au(001) along $\bar{\Gamma} - \bar{X}$. Bright and dark colors represent large and small values of DOS, respectively, with the color scale being linear with $\log_{10}$(DOS). (b) y component of k-resolved spin DOS calculated in a first-layer MT sphere for semi-infinite Au(001) along $\bar{\Gamma} - \bar{X}$. Red and blue colors correspond to spin polarization parallel and antiparallel to the y axis, respectively. (c) k-resolved DOS and (d) y component of k-resolved spin DOS in a smaller region near the band-gap minimum calculated with finer energy and k mesh points.

than) ω that ΔE_{SO} essentially agrees with ΔE_{CD}. We would like to note that it is particularly important to take into account the difference when the intensity asymmetry is not so large. The right panel of Fig. 7 indicates that $\Delta E_{\mathrm{CD}} = \Delta E_{SO}$ only when $I_\uparrow : I_\downarrow = 1 : 0$, which is unrealistic. For the correct determination of the Rashba parameter, it is necessary to analyze the dependence of ΔE_{CD} on the momentum at multiple emission angles.

APPENDIX B: TOPOLOGICAL STATES

Figure 8(a) shows the wide range intensity plot of the k-resolved DOS along the $\bar{\Gamma} - \bar{X}$ line. Figure 8(b) shows the y component of the k-resolved spin DOS calculated in the same MT sphere. Here, the x and y axes are parallel to the two sides of a square unit cell of the 1×1 lattice, and parallel momentum $k_\parallel$ is oriented in the positive x direction. Discrete energy bands appearing inside the projected band gap are localized surface states. Aside from the full series of IPSs, we find a pair of Shockley states degenerate at the $\bar{\Gamma}$ point (α) and also three pairs degenerate at the $\bar{X}$ point (β, γ, δ). All of these surface bands exhibit Rashba splitting as $k_\parallel$ deviates from $\bar{\Gamma}$ or $\bar{X}$. Furthermore, as seen from Fig. 8(b), the electron spins of these bands are polarized either parallel or antiparallel to the y axis, with the two states in each pair having opposite spin directions.

In a recent paper [40], Yan *et al.* revealed that the band structure of fcc Au is topologically nontrivial if the lowest twelve energy bands (including spin degrees of freedom) are regarded as "valence bands" separated from the higher ones ("conduction bands") by a nonvanishing direct energy gap in the entire bulk Brillouin zone. Based on this idea, it was claimed that the partially occupied L-gap surface states on Au(111) may be regarded as a topological surface band. However, strictly speaking, topological classification of surface bands is possible only when the direct band gap along a path connecting two time-reversal invariant momentum points is positive all along the line. In this sense, Au(001) is more suitable than Au(111) for examining the topological property of the band structure, since Au(001) has a finite direct band gap throughout the $\bar{\Gamma} - \bar{X}$ line, while the projected bulk band gap of Au(111) is closed in the middle of the $\bar{\Gamma} - \bar{\mathrm{M}}$ line.

A hallmark of topological insulators is the existence of "metallic" surface bands whose energy dispersion with k crosses a projected bulk band gap, thus connecting the "valence" and "conduction" bands. It is seen from Fig. 8 that the image potential states do not have topological nature because their energy dispersion curves are merged into the upper projected bulk bands on the higher-energy side of the band gap. Similarly, the δ band is not topological. To examine if the other Shockley surface states have topological origin or not, we calculated the k-resolved DOS and the y component of the spin DOS in a small interval around $k_{\parallel} \sim 0.71\ \text{Å}^{-1}$, where the projected bulk band gap becomes the smallest, by using finer energy and k mesh points [see Figs. 8(c) and 8(d)]. As seen from these figures, the upper branch of both the β and γ bands is merged into the upper projected bulk bands, while their lower branch is merged into the lower ones. Thus, both bands can be regarded as topological surface bands. Here, we note that the lower branch of the β band and the upper branch of the γ band cross each other without interactions because of different symmetries. The behavior of the α band is more complicated. Starting from the $\bar{\Gamma}$ point, its lower branch is merged into the lower projected bulk bands at $k_{\parallel} \sim 0.27\ \text{Å}^{-1}$. Its upper branch, which persists beyond this $k_{\parallel}$ value, is once merged into the lower projected bulk bands at $k_{\parallel} \sim 0.35\ \text{Å}^{-1}$. However, the upper branch is again split from the bulk band at $k_{\parallel} \sim 0.46\ \text{Å}^{-1}$ and crosses the band gap until it is finally merged into the upper projected bulk bands. Since the α band connects the "valence" and "conduction" bands, its energy dispersion may have also topological origin. Now, consider an arbitrary line, $E = E(k_{\parallel})$, passing in the interior of the projected bulk band gap from $\bar{\Gamma}$ to $\bar{\mathrm{X}}$. Then, one will see that the number of surface bands crossing this line is always odd (3, 5,...) in agreement with the finding of Yan *et al.* [40] that the band structure of Au is topologically nontrivial. If one of the α, β, and γ bands did not cross the band gap, this number would become even, which contradicts their theoretical prediction.

[1] Y. A. Bychkov and E. I. Rashba, JETP Lett. **39**, 78 (1984).

[2] S. A. Wolf, D. D. Awschalom, R. A. Buhrman, J. M. Daughton, S. von Molnár, M. L. Roukes, A. Y. Chtchelkanova, and D. M. Treger, Science **294**, 1488 (2001).

[3] R. Winkler, *Spin-Orbit Coupling Effects in Two-Dimensional Electron and Hole Systems* (Springer, Berlin, 2003).

[4] G. Bihlmayer, O. Rader, and R. Winkler, New J. Phys. **17**, 50202 (2015).

[5] E. E. Krasovskii, J. Phys.: Condens. Matter **27**, 493001 (2015).

[6] S. Datta and B. Das, Appl. Phys. Lett. **56**, 665 (1990).

[7] C. Jozwiak, C.-H. Park, K. Gotlieb, C. Hwang, D.-H. Lee, S. G. Louie, J. D. Denlinger, C. R. Rotundu, R. J. Birgeneau, Z. Hussain, and A. Lanzara, Nat. Phys. **9**, 293 (2013).

[8] C. Kastl, C. Karnetzky, H. Karl, and A. W. Holleitner, Nat. Commun. **6**, 6617 (2015).

[9] D. Hsieh, Y. Xia, D. Qian, L. Wray, J. H. Dil, F. Meier, J. Osterwalder, L. Patthey, J. G. Checkelsky, N. P. Ong, A. V. Fedorov, H. Lin, A. Bansil, D. Grauer, Y. S. Hor, R. J. Cava, and M. Z. Hasan, Nature (London) **460**, 1101 (2009).

[10] J. W. McIver, D. Hsieh, H. Steinberg, P. Jarillo-Herrero, and N. Gedik, Nat. Nanotechnol. **7**, 96 (2012).

[11] A. Junck, G. Refael, and F. von Oppen, Phys. Rev. B **88**, 075144 (2013).

[12] J. Sánchez-Barriga, A. Varykhalov, J. Braun, S.-Y. Xu, N. Alidoust, O. Kornilov, J. Minár, K. Hummer, G. Springholz, G. Bauer, R. Schumann, L. V. Yashina, H. Ebert, M. Z. Hasan, and O. Rader, Phys. Rev. X **4**, 011046 (2014).

[13] U. Höfer, I. L. Shumay, C. Reuß, U. Thomann, W. Wallauer, and T. Fauster, Science **277**, 1480 (1997).

[14] J. Güdde, M. Rohleder, T. Meier, S. W. Koch, and U. Höfer, Science **318**, 1287 (2007).

[15] M. Weinelt, J. Phys.: Condens. Matter **14**, R1099 (2002).

[16] U. Bovensiepen, H. Petek, and M. Wolf, *Dynamics at Solid State Surfaces and Interfaces*, Vol. 1, Current Developments (Wiley-VCH, Weinheim, Germany, 2010).

[17] S. Tognolini, S. Achilli, L. Longetti, E. Fava, C. Mariani, M. I. Trioni, and S. Pagliara, Phys. Rev. Lett. **115**, 046801 (2015).

[18] D. Niesner, T. Fauster, S. V. Eremeev, T. V. Menshchikova, Y. M. Koroteev, A. P. Protogenov, E. V. Chulkov, O. E. Tereshchenko, K. A. Kokh, O. Alekperov, A. Nadjafov, and N. Mamedov, Phys. Rev. B **86**, 205403 (2012).

[19] D. Niesner, S. Otto, T. Fauster, E. V. Chulkov, S. V. Eremeev, O. E. Tereshchenko, and K. A. Kokh, J. Electron Spectrosc. Relat. Phenom. **195**, 258 (2014).

[20] A. B. Schmidt, M. Pickel, M. Wiemhöfer, M. Donath, and M. Weinelt, Phys. Rev. Lett. **95**, 107402 (2005).

[21] M. Donath, C. Math, M. Pickel, A. B. Schmidt, and M. Weinelt, Surf. Sci. **601**, 5701 (2007).

[22] M. Weinelt, A. B. Schmidt, M. Pickel, and M. Donath, Prog. Surf. Sci. **82**, 388 (2007).

[23] A. Winkelmann, F. Bisio, R. Ocaña, W.-C. Lin, M. Nývlt, H. Petek, and J. Kirschner, Phys. Rev. Lett. **98**, 226601 (2007).

[24] M. Pickel, A. B. Schmidt, M. Weinelt, and M. Donath, Phys. Rev. Lett. **104**, 237204 (2010).

[25] F. Passek and M. Donath, Phys. Rev. Lett. **69**, 1101 (1992).

[26] S. D. Stolwijk, A. B. Schmidt, M. Donath, K. Sakamoto, and P. Krüger, Phys. Rev. Lett. **111**, 176402 (2013).

[27] S. N. P. Wissing, A. B. Schmidt, H. Mirhosseini, J. Henk, C. R. Ast, and M. Donath, Phys. Rev. Lett. **113**, 116402 (2014).
[28] K. Hild, J. Maul, G. Schönhense, H. J. Elmers, M. Amft, and P. M. Oppeneer, Phys. Rev. Lett. **102**, 057207 (2009).
[29] C.-T. Chiang, A. Winkelmann, P. Yu, and J. Kirschner, Phys. Rev. Lett. **103**, 077601 (2009).
[30] P. M. Echenique and J. B. Pendry, J. Phys. C **11**, 2065 (1978).
[31] T. Fauster, M. Weinelt, and U. Höfer, Prog. Surf. Sci. **82**, 224 (2007).
[32] S. LaShell, B. A. McDougall, and E. Jensen, Phys. Rev. Lett. **77**, 3419 (1996).
[33] M. Hoesch, M. Muntwiler, V. N. Petrov, M. Hengsberger, L. Patthey, M. Shi, M. Falub, T. Greber, and J. Osterwalder, Phys. Rev. B **69**, 241401 (2004).
[34] J. R. McLaughlan, E. M. Llewellyn-Samuel, and S. Crampin, J. Phys.: Condens. Matter **16**, 6841 (2004).
[35] H. Cercellier, C. Didiot, Y. Fagot-Revurat, B. Kierren, L. Moreau, D. Malterre, and F. Reinert, Phys. Rev. B **73**, 195413 (2006).
[36] A. Tamai, W. Meevasana, P. D. C. King, C. W. Nicholson, A. de la Torre, E. Rozbicki, and F. Baumberger, Phys. Rev. B **87**, 075113 (2013).
[37] A. Varykhalov, D. Marchenko, M. R. Scholz, E. D. L. Rienks, T. K. Kim, G. Bihlmayer, J. Sánchez-Barriga, and O. Rader, Phys. Rev. Lett. **108**, 066804 (2012).
[38] B. Kim, C. H. Kim, P. Kim, W. Jung, Y. Kim, Y. Koh, M. Arita, K. Shimada, H. Namatame, M. Taniguchi, J. Yu, and C. Kim, Phys. Rev. B **85**, 195402 (2012).
[39] H. Ishida, Phys. Rev. B **90**, 235422 (2014).
[40] B. Yan, B. Stadtmüller, N. Haag, S. Jakobs, J. Seidel, D. Jungkenn, S. Mathias, M. Cinchetti, M. Aeschlimann, and C. Felser, Nat. Commun. **6**, 10167 (2015).
[41] H. Ishida, Phys. Rev. B **63**, 165409 (2001).
[42] H. Ishida, Y. Hamamoto, Y. Morikawa, E. Minamitani, R. Arafune, and N. Takagi, New J. Phys. **17**, 15013 (2015).
[43] T. Yokoyama, T. Nakagawa, and Y. Takagi, Int. Rev. Phys. Chem. **27**, 449 (2008).
[44] J. E. Inglesfield, J. Phys. C **14**, 3795 (1981).
[45] D. J. Singh and L. Nordstrom, *Planewaves, Pseudopotentials, and the LAPW Method*, 2nd ed. (Springer, Berlin, 2006).
[46] G. Butti, S. Caravati, G. P. Brivio, M. I. Trioni, and H. Ishida, Phys. Rev. B **72**, 125402 (2005).
[47] D. Straub and F. J. Himpsel, Phys. Rev. B **33**, 2256 (1986).
[48] G. V. Hansson and S. A. Flodström, Phys. Rev. B **18**, 1572 (1978).
[49] F. Ciccacci, S. D. Rossi, A. Taglia, and S. Crampin, J. Phys.: Condens. Matter **6**, 7227 (1994).
[50] U. Thomann, C. Reuß, T. Fauster, F. Passek, and M. Donath, Phys. Rev. B **61**, 16163 (2000).